Journal of Magnetism and Magnetic Materials 0 (2009) 1–0

Contents lists available at ScienceDirect

Journal of Magnetism and Magnetic Materials

journal homepage: www.elsevier.com/locate/jmmm

Optimization of Electromagnet for High–Field Polar Magneto–Optical Microscopy

D. Lukáš [a,*], K. Postava [b], O. Životský [b], J. Pištora [b]

[a] Department of Applied Mathematics, Technical University of Ostrava, 17. listopadu 15, 708 33 Ostrava–Poruba, Czech Republic
[b] Department of Physics, Technical University of Ostrava, 17. listopadu 15, 708 33 Ostrava–Poruba, Czech Republic

ARTICLE INFO

PACS:
02.70.Dh;
02.70.Pt;
02.60.Pn;
68.37.-d

Keywords:
electromagnet
optimization; Kerr
microscopy;
nonlinear
magnetostatics;
boundary elements

ABSTRACT

In this paper we propose a new method for simulation and optimization of the field of electromagnets. The method is applied to optimize the polar electromagnet with cylindrical symmetry for magneto-optic microscopy. The direct simulation is based on a discretization of Maxwell's equations by means of finite elements in the interior ferromagnetic parts that are coupled with boundary elements to model the exterior field. The ferromagnetic nonlinearity is treated by the Newton method. Further, we optimize shape of the ferromagnetics in order to achieve magnetic field above a pole head as high and as homogeneous as possible. The example of optimized electromagnet fits to a compact Zeiss polarization microscope adapted for polar magneto-optic domain visualization. Within the optimization we achieved the magnetic field of 0.23 T with inhomogeneity of 6 % in a nonsaturated regime when applying a lower electric current, while in a saturated regime with a higher current applied the magnetic field was 0.47 T with inhomogeneity lower than 6 %.

1. Introduction

Magneto-optical Kerr microscopy is an efficient, nondestructive, and noninvasive method for local observation of magnetic domains [1–3] and two-dimensional maps of local hysteresis loops [4]. Similarly, characterization of advanced nanostructures produced by lithography requires focusing of inspected optical beam into the sufficiently small spot. For both applications the objective optics is in the vicinity of a sample and therefore influence of magnetic field on focusing objective have to be minimized. Hence there is a need to design efficient electromagnets generating high and homogeneous magnetic field in the area of the sample and simultaneously minimize magnetic field near the objective.

In order to model and optimize magnetic field of such an electromagnet, we consider the magnetostatic case of Maxwell's equations. To solve the model numerically, the finite element method (FEM) is usually employed [5,6]. However, FEM introduces an artificial truncation of the computational domain far enough from both the ferromagnetic parts and the currents, which increases size of the resulting algebraic system. Additionally, within shape optimization one has to deform the discretization grid not only in the ferromagnetics, but in the exterior too.

To solve this problem we propose a method that combines the traditional FEM with the boundary elements method (BEM). The FEM-BEM combination takes the advantage of both methods, i.e. possibility to model the ferromagnetic nonlinearities as well as the exterior magnetic field. The coupling scheme was originally proposed and rigorously analyzed in [8] to solve the eddy current problems. A novelty of this paper is that we apply the latter scheme to a problem of optimal shape design governed with the nonlinear magnetostatics.

2. Mathematical modeling and optimization

Process of the magnetic field simulation and optimization can be divided into three main steps, described in details in Sections 2.1, 2.2, and 2.3. In the first step we define a mathematical model using the differential Maxwell's equations for the vector potential $\mathbf{A}$ in the specific regions of the electromagnet as well as related boundary conditions. In the next step we propose to couple the Newton method and FEM in order to model the nonlinear behavior in ferromagnetics [8]. Moreover, by adding BEM, we ensure that the exterior field is correctly modeled via a convolution of boundary potentials with a known fundamental solution. Thus, no domain truncation nor an inner discretization is needed. The price for that is a considerably more implementation effort and the fact that the resulting system matrices are densely populated. Finally, in Section 2.3, a shape optimization problem for the electromagnet shape design is introduced.

2.1. Mathematical model

As a model we consider the following nonlinear magnetostatic case of Maxwell's equations, where we refer to Fig. 1 for the notation:

$$\nabla \times \mathbf{H}^i = 0 \text{ in } \Omega^i, \tag{1}$$

$$\nabla \times \mathbf{H}^e = \mathbf{J} \text{ in } \Omega^e_J, \tag{2}$$

$$\nabla \times \mathbf{H}^e = 0 \text{ in } \Omega^e \setminus \overline{\Omega_J}, \tag{3}$$

* Corresponding author.
Email address: dalibor.lukas@vsb.cz (D. Lukáš).

0304-8853/09/$ - see frontmatter

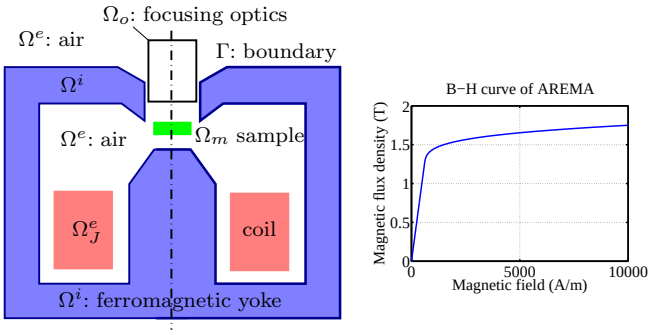

Fig. 1. Scheme of the axisymmetric electromagnet. Right subplot shows B–H curve of the typical soft magnetic iron 'AREMA' used in modeling here.

$$\nabla \cdot \mathbf{B}^i = 0 \text{ in } \Omega^i, \tag{4}$$

$$\nabla \cdot \mathbf{B}^e = 0 \text{ in } \Omega^e, \tag{5}$$

where $\mathbf{H}^i$ and $\mathbf{H}^e$ denotes the magnetic intensity in the ferromagnetic yoke domain Ω^i and in the remainder $\Omega^e := \mathbb{R}^3 \setminus \overline{\Omega^i}$, respectively, where further $\mathbf{B}^i$ and $\mathbf{B}^e$ denotes the magnetic flux density in Ω^i and Ω^e, respectively. The coil occupies the domain Ω_J^e and it is pumped with the current density $\mathbf{J}$. Moreover, we consider nonlinear ferromagnetic behavior in Ω^i: $\mathbf{B}^i = \mu(|\mathbf{B}^i|)\,\mathbf{H}^i$, see Fig. 1, where μ is the nonlinear permeability function. Similarly in Ω^e: $\mathbf{B}^e = \mu_0\,\mathbf{H}^e$ holds, where μ_0 is the permeability of vacuum (air). Further, we prescribe at least quadratic decay of the magnetic field at infinity. To complete the model, we have to couple the magnetic field in Ω^i and Ω^e via the transmission conditions:

$$\mathbf{n} \cdot (\mathbf{B}^i - \mathbf{B}^e) = 0 \qquad \text{on } \Gamma, \tag{6}$$

$$\mathbf{n} \times (\mathbf{H}^i - \mathbf{H}^e) = 0 \qquad \text{on } \Gamma \tag{7}$$

where $\Gamma := \partial\Omega^i$ is the boundary between the ferromagnetic yoke and nonmagnetic surrounding, see Fig. 1, and where $\mathbf{n}$ denotes the outward unit normal vector to Ω^i. Finally, we introduce the magnetic vector potentials $\mathbf{A}^i$ in Ω^i and $\mathbf{A}^e$ in Ω^e such that $\nabla \times \mathbf{A}^i = \mathbf{B}^i$ and $\nabla \times \mathbf{A}^e = \mathbf{B}^e$, respectively. Then (4) and (5) are automatically fulfilled and from (1)–(3) we get a system of second–order partial differential equations (PDE), the solution to which is mathematically better understood, cf. [6], than the original first–order PDE system (1)–(5).

2.2. Combined FEM–BEM method

The FEM formulation of our problem is based on minimization of the following energy functional:

$$E(\mathbf{A}^i, \mathbf{A}^e) = \frac{1}{2}\int_{\Omega^i} \mu(|\nabla \times \mathbf{A}^i|)^{-1} \left|\nabla \times \mathbf{A}^i\right|^2 dx + \frac{1}{2}\int_{\Omega^e} \mu_0^{-1} |\nabla \times \mathbf{A}^e|^2 \, dx - \int_{\Omega_J} \mathbf{J} \cdot \mathbf{A}^e \, dx, \tag{8}$$

which can easily treat nonlinearities by employing e.g. the Newton method. However, the domain Ω^e has to be truncated and the decay at infinity is replaced by $\mathbf{A}^e \times \mathbf{n}^e = 0$ along the new truncated part of the boundary of Ω^e, where $\mathbf{n}^e$ is the related unit outward normal. Moreover, even for slow computation with a lot of extra unknowns, the precision is limited by truncation.

On the other hand, the BEM formulation is based on an exact integral representation of both $\mathbf{A}^i$ and $\mathbf{A}^e$, which is due to Stratton and Chu in case of Maxwell's equations [10]. For the latter we need to know the so–called boundary potentials defined on the interface Γ, which we get by solution to the transmission equations (6)–(7) while the remaining equations of the model are fulfilled automatically. However, BEM assumes only linear materials, i.e. $\mu(|\mathbf{B}^i|)$ is a constant. In such a case, we only have to mesh the interface, which leads to a significant reduction of the computational time, comparing to FEM, when solving the model.

A nice feature of FEM and BEM is that they can be very naturally coupled so that we can make use of resolving the nonlinear B–H curve behavior by FEM and resolving the infinity decay conditions by BEM. For a detail description and rigorous analysis of this coupling we refer the reader to [8,9]. Note that we only have to discretize the ferromagnetic yoke domain Ω^i.

2.3. Shape optimization

We are actually interested in an optimal design of the electromagnet. Namely, we wish the magnetic field to be as homogeneous as possible in the sample-location volume Ω_m while keeping it large enough there and small enough in the volume of focusing optics Ω_o, see Fig. 1. To this end, we first solve the following optimization subproblem:

$$\max B_z^{avg}, \tag{9}$$

where B_z^{avg} is the axial component of the average magnetic flux density of $\mathbf{B}^e$ over Ω_m. Further, we try to keep 80% of improvements of the magnetic flux magnitude with respect to an initial design and we aim at the forthcoming optimization:

$$\min \left\{ \kappa/\kappa_{opt} + |\mathbf{B}_o^{avg}|/B_{opt} \right\}, \tag{10}$$

where $\mathbf{B}_o^{avg}$ is the average magnetic flux density over the volume of focusing optics Ω_o and κ is the square root of the standard deviation of $\mathbf{B}^e$ from $(0, 0, B_z^{avg})$ over the sample volume Ω_m, both divided by the volume of Ω_o and that of Ω_m, respectively. The first and the second term of Eq. (10) lead to increase field homogeneity and minimize the field in the focusing optics volume, respectively. We optimize over the shapes of the ferromagnetic yoke boundary Γ. The optimization is performed using a quasi–Newton optimization method [11].

3. Results and discussion

The general method proposed in the previous section is applied to shape optimization of the axisymmetric electromagnet, which produces a polar magnetic field. The optimization was performed for the current of 1 A when considering 3280 turns with the wire diameter of 0.7 mm and total resistance of 7 Ω. We achieved the magnetic field $B^{avg} = 0.230$ T with inhomogeneities of 6 % in the sample area, while close to the focusing optics the field was minimized to 12 mT. Figure 2 shows the optimized magnet shape with the sample arrows of the magnetic flux density (left subplot) and the magnetic flux magnitude (right subplot).

Further, we are interested in the magnetic field when applying the current 4 A to the same optimized configuration. This corresponds to maximal current obtained by standard power supply 400 W and a water cooled coil. Right subplot of Fig. 3 shows the corresponding magnetic flux density maps, where in the left subplot we show the homogeneity of the magnetic flux density in Ω_m and its decay in Ω_o as

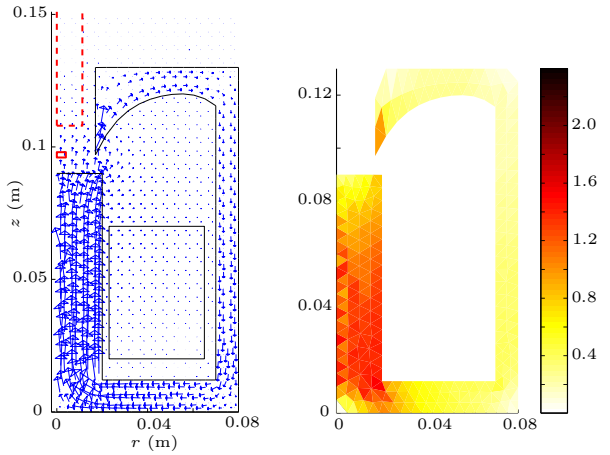

Fig. 2. Optimal axisymmetric shape with the sample Ω_m and optics Ω_o volume are plotted together with arrows of the magnetic flux density (left subplot). The amplitudes of the magnetic flux density $|\mathbf{B}|$ (T) for the excitation current of 1 A is shown (right subplot).

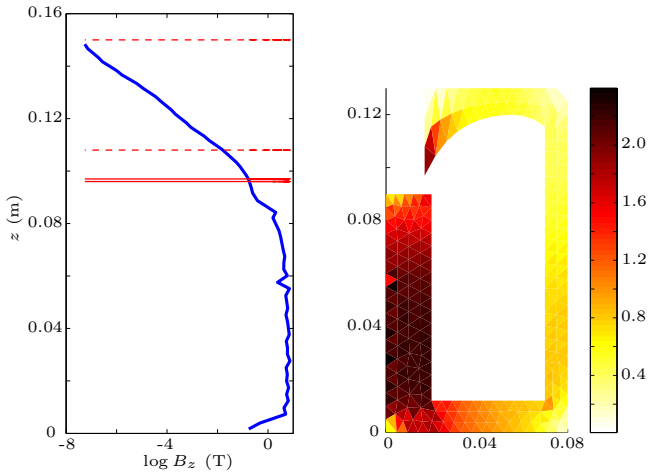

Fig. 3. The amplitude of magnetic flux density$|\mathbf{B}|$ (T) for the excitation current of 4 A is shown on the right subplot. The left subplot shows decrease of the axial magnetic flux component on the electromagnet axis in the logarithmic scale.

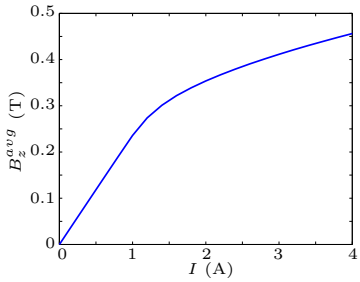

Fig. 4. Dependence of B_z^{avg} on the excitation current I.

solid and dashed rectangles, respectively. For this setting we achieved the magnetic field $B^{avg} = 0.468\,\mathrm{T}$ with 5.8 % inhomogeneities. The magnetic field in the focusing optics is 26 mT. Next, we refer to Fig. 4, where a dependence of the magnetic field B^{avg} on the excitation current I is plotted. We can see that for currents higher than 1 A, indeed, the excitation becomes less efficient due to the saturation.

Finally, we briefly describe some computational aspects of the optimization. We consider 16 design parameters that are vertical displacements of Bézier nodes controlling the shape of the pole head (3), of the cover bottom part (6) and of the cover top part (6), together with nonpenetration conditions. The optimization subproblem (9) took 32 quasi–Newton iterations and the following minimization (10) finished in 3 quasi–Newton iterations. The most time consuming part is direct simulation of the magnetic field for a given design, which was done using 125 boundary unknowns along Γ and 266 inner nodal unknowns in Ω^i, i.e. 491 unknowns in total. We have experienced that simulation by pure FEM needs to place the artificial truncation boundary at about 5 times further behind the ferromagnetics which corresponds to an expectation that the overall computational time of the pure FEM–based optimization will be 5 times longer with yet a less reliable result. Moreover, one would have to deal with deformation of the exterior domain and remesh the discretization grid a couple of times.

4. Conclusion

We conclude by summarizing advantages of the proposed optimization algorithm based on combination of the finite elements and boundary elements methods (FEM–BEM): (i) nonlinear response of the ferromagnetic yoke (nonlinear permeability μ) is included, (ii) combined FEM-BEM algorithm enables an effective computation and eliminates the FEM–error arising from the domain truncation, (iii) avoids the troubles with a deformation of the FEM grid in the electromagnet exterior within the shape optimization, and, finally, (iv) by using multigrid techniques and hierarchical matrices the algorithm can be extended to become an extremely efficient solution technique for large–scale simulations as well as optimization problems.

Acknowledgment

This work was supported by the Czech Ministry of Education under the project MSM6198910027 and by the Czech Academy of Science under the project AVČR 1ET400300415. Partial support from the project KAN 400100653 and from the Grant Agency of the Czech Republic (202/06/0531) is acknowledged.

References

[1] A. Hubert and R. Schäfer, *Magnetic domains: the analysis of magnetic microstructures* (Springer, Berlin, 1998).
[2] R. Schäfer, In: *Handbook of Magnetism and Advanced Magnetic Materials* (John Willey & Sons, Berlin, 2007).
[3] M. Kisielewski, A. Maziewski, M. Tekielak, J. Ferré, S. Lemerle, V. Mathet, C. Chappert, J. Magn. Magn. Mater. 260 (2003) 231.
[4] S.-B. Choe and D.-H. Kim and Y.-C. Cho and H.-J. Jang and K.-S. Ryu and H.-S. Lee and S.-C. Shin, Rev. Sci. Instrum. 73 (2002) 2910.
[5] Comsol Multiphysics modelling *http://www.comsol.com*; ANSYS, Inc. Software Products *http://www.ansys.com*.
[6] A. Bossavit, *Computational Electromagnetism. Variational Formulations, Complementarity, Edge Elements* (Orlando, FL, Academic Press, 1998).
[7] J. Haslinger and R.A.E. Mäkinen, *Introduction to Shape Optimization. Theory, Approximation, and Computation* (SIAM, Philadelphia 2003).
[8] R. Hiptmair, Symmetric coupling for eddy current problems. SIAM J. Numer. Anal. **40** (2002) 41–65.
[9] D. Lukáš, K. Postava, O. Životský, A Shape optimization method in nonlinear axisymmetric magnetostatics using a coupling of finite and boundary elements (submitted to J. Sci. Comp.).
[10] J.-C. Nédélec, *Acoustic and Electromagnetic Equations, Integral Representations for Harmonic Problems* (Springer–Verlag New York, Berlin, Heidelberg, 2001).
[11] W. H. Press, S. A. Teukolsky, W. T. Vetterling and B. P. Flannery, *Numerical Recipes in C – The Art of Scientific Computing* (Cambridge University Press, 1997).